ARTICLES

Comparison of keV $N_2^{+\bullet}$/He and $N_2^{+\bullet}$/Ar Collisions by Emission Spectroscopy and Theory

Clement Poon, Yawei Lin, and Paul M. Mayer*

Department of Chemistry, University of Ottawa, 10 Marie-Curie, Ottawa, Ontario, Canada K1N 6N5

Received: February 28, 2008; Revised Manuscript Received: June 9, 2008

Collision-induced emission spectra from 190−1020 nm were obtained for $N_2^{+\bullet}$/Ar collisions at laboratory frame collision energies from 2 to 8 keV. The relative emission intensities of $N_2^{+\bullet}$, N^+, and $N^\bullet$ are independent of the ion translational energy within the studied energy range, supporting the curve-crossing mechanism for collisional excitation. The role of the target gas in keV $N_2^{+\bullet}$/He and $N_2^{+\bullet}$/Ar collisions was investigated by both emission spectroscopy and theoretical calculations. Adiabatic potential energy surfaces calculated at the CISD/6-311+G(2df) level of theory for $N_2^{+\bullet}$/He and $N_2^{+\bullet}$/Ar collisions indicate that excitation to the A $^2\Pi_u$ and B $^2\Sigma_u^+$ states involves curve-crossing first to the C $^2\Sigma_u^+$ state, and the difference in $N_2^{+\bullet}$ emission intensities from the two systems can be accounted for by the slope difference at the crossing points based on the Landau−Zener curve-crossing model.

1. Introduction

Collision-induced dissociation (CID) is an important tool in mass spectrometry for elucidating ion structures.[1–4] This process is often considered a two-step process, in which the first step excites the ions by collision, converting some of the ion translational energy into internal energy. This is followed by a second step involving dissociation of ions containing energy above the dissociation threshold. Our interest is to use emission spectroscopy to probe internal excitation in keV ion-target collisions to obtain information on the first step of the two-step process.

In the keV laboratory-frame collision energy range, excitation by momentum transfer is minimized. As a result, collisional activation at this energy range normally involves only electronic excitation. Two mechanisms, vertical transitions and curve crossings, have been proposed for keV collisions.[5,6]

In contrast to photoexcitation, in which a precise energy determined by the wavelength of the light source is deposited into the precursor ions, collisions deposit a range of energies. Therefore, when the vertical transition model is applied for collisional excitation, it is assumed that electronic transitions to various excited states take place simultaneously and in competition with each other. As a result, higher ion translational energy (i.e., higher ion velocity) should favor higher-energy transitions. Relatively stronger emissions would then be expected from species formed at higher internal energy (such as excited-state fragments).

However, when collisional activation occurs via curve crossings, transitions occur at a few curve-crossing points and may then be followed by a complicated sequence of nonadiabatic interactions. Figure 1 illustrates two potential energy curves ($V_i(r)$ and $V_f(r)$) representing the initial and the final electronic states of a polyatomic collision complex. Based on the Landau−Zener model,[7] the probability (P) of crossing-over at a crossing point can be reflected in terms of the slope (dV/dr) difference at the crossing point and the relative velocity (v) of the two colliding species:

$$P = e^{-2\delta} \quad \text{where} \quad \delta = \frac{(2\pi)^{3/2} H_{12}^{\,2}(R)}{\left(\left|\frac{dV_1}{dr} - \frac{dV_2}{dr}\right|\right) h v} \qquad (1)$$

where H_{12} is the off diagonal matrix element describing the transition between two electronic states (1 and 2), and h is Planck's constant.[8–10] Higher ion translational energy will increase the probability that the system will cross to another electronic state, but the distribution of the excited states of the collision complex generated could remain constant. For a polyatomic system as in the present study, a two-dimensional extension of LZ theory is required,[9,10] but eq 1 still gives a qualitative picture of what will be important governing factors for the transition probability in the present study.

There are two major approaches to the study of collisional activation that allow us to identify the final electronic states resulting from collisions. One of them is translational energy spectroscopy (TES),[11] in which the amount of translational energy being converted into internal energy is directly measured. This technique has been used to study a number of collisions involving different diatomic ions or molecules. A recent study by Fuentes and Martinez[12] and a previous study by Fournier et

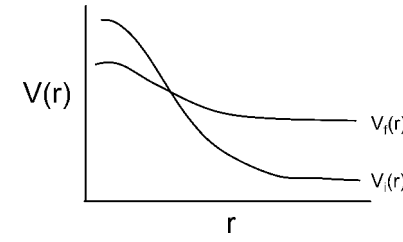

Figure 1. Two-dimensional diagram illustrating crossing of potential energy curves of a polyatomic collision complex.

* Corresponding author. Tel: (613) 562-5800, ext. 6038. Fax: (613) 562-5170. E-mail: pmmayer@uottawa.ca.

10.1021/jp8017524 CCC: $40.75
Published on Web 08/05/2008

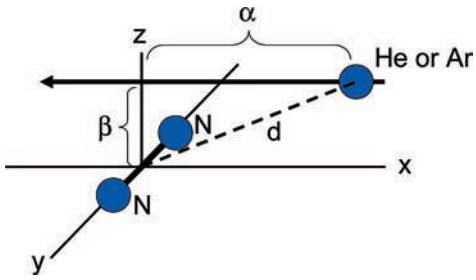

Figure 2. Collision trajectory between a target atom (He or Ar) and a $N_2^{+\bullet}$ ion used in this study.

TABLE 1: Observed Emissions in Figures 3 and 4 and Their Corresponding Radiative Lifetimes

transition			τ (ns)[a]	λ (nm)	refs
$N_2^{+\bullet}$	B $^2\Sigma_u^+ \rightarrow$ X $^2\Sigma_g^+$	$\Delta v = +2$	~60	332	25–27
		$\Delta v = +1$		356	
		$\Delta v = 0$		390	
		$\Delta v = -1$		424	
		$\Delta v = -2$		465	
N_2	C $^3\Pi_u \rightarrow$ B $^3\Pi_g$	$\Delta v = +2$	~39	296	27, 28
		$\Delta v = +1$		314	
		$\Delta v = 0$		333	
		$\Delta v = -1$		352	
		$\Delta v = -2$		376	
N^+	(3d) $^3F^0 \rightarrow$ (3p) ^3D		8	503	29, 30
	(3p) $^3S \rightarrow$ (3s) $^3P^0$		13	503	
	(3p) $^3D \rightarrow$ (3s) $^3P^0$		18	570	
N	(3p) $^2D^0 \rightarrow$ (3s) ^2P		46	941	29, 30
Ar	$(4p')[1/2]_1 \rightarrow (4s)[3/2]_2$		149	697	29–31
	$(4p')[3/2]_2 \rightarrow (4s)[3/2]_2$		253	707	
	$(4p')[3/2]_2 \rightarrow (4s)[3/2]_1$			738	
	$(4p)[1/2]_0 \rightarrow (4s)[3/2]_1$		21	752	
	$(4p)[3/2]_2 \rightarrow (4s)[3/2]_2$			773	
	$(4p)[3/2]_1 \rightarrow (4s)[3/2]_2$			802	
	$(4p)[5/2]_2 \rightarrow (4s)[3/2]_2$		108		
Ar	$(4p)[5/2]_3 \rightarrow (4s)[3/2]_2$		30	812	
	$(4p')[1/2]_1 \rightarrow (4s')[1/2]_1$			826	
	$(4p)[5/2]_2 \rightarrow (4s)[3/2]_1$			843	
	$(4p')[3/2]_1 \rightarrow (4s')[1/2]_1$			853	
	$(4p)[3/2]_1 \rightarrow (4s')[1/2]_0$			868	
	$(4p)[1/2]_1 \rightarrow (4s)[3/2]_2$		53	913	
	$(4p)[3/2]_1 \rightarrow (4s')[1/2]_1$			922	

[a] Lifetimes from refs 25, 26, 28, and 30.

TABLE 2: Emission Intensity (in Photon Counts) of the $\Delta v = +1$ (356 nm) and $\Delta v = 0$ (390 nm) Transitions of $N_2^{+\bullet}$ B $^2\Sigma_u^+ \rightarrow$ X $^2\Sigma_g^+$ from 8 keV $N_2^{+\bullet}$/He and $N_2^{+\bullet}$/Ar Collisions

	$N_2^{+\bullet}$/He		$N_2^{+\bullet}$/Ar	
accumulation time	I (356 nm)	I (390 nm)	I (356 nm)	I (390 nm)
30 min	391	721	173	165
1 h	698	1247	384	364

al.[13] on $N_2^{+\bullet}$/He collisions suggest that upon collisions N^+ is produced from the C $^2\Sigma_u^+$ and the D $^2\Pi_g$ states of $N_2^{+\bullet}$. Comparison of the TES spectra of keV $N_2^{+\bullet}$/He and $N_2^{+\bullet}$/Ar collisions suggested that dissociation from the D $^2\Pi_g$ state is relatively more important when Ar is the target than for a He target.[12]

The other experimental strategy is by observing photon emissions from collisionally activated species.[14] This method, sometimes referred to as collision-induced emission (CIE) spectroscopy, has the advantage of higher resolution and higher sensitivity. Our earlier study[15] on the keV $N_2^{+\bullet}$/He collisions by CIE spectroscopy showed that the relative emission intensity resulting from $N^\bullet$ and N^+ fragments and the precursor $N_2^{+\bullet}$ ions

TABLE 3: Slope Difference at Crossing Points of the Potential Energy Curves Calculated at the CISD/6-311+G(2df) and TD B3-LYP/6-311+G(2df) Levels of Theory

	slope difference at crossing points (eV Å^{-1})		
β (Å)	X → C	C → A	C → B
$N_2^{+\bullet}$/He			
TD B3-LYP			
0.8	13	18	6
CISD			
0.5	20	19	7
0.6	17	21	8
0.7	15	17	6
0.8	18	15	6
av	18	18	6
$N_2^{+\bullet}$/Ar			
CISD			
1.0	10	10	8
1.1	9	10	6
1.2	9	9	6
1.3	9	8	5
1.4	6	8	6
av	9	9	6

are independent of the ion translational energy within the keV collision energy range, suggesting that collisional excitation involves curve crossings rather than vertical transitions. We have extended this study to include collisions involving a heavier target gas, Ar. In the present article, we will present results from our study of keV $N_2^{+\bullet}$/Ar collisions by emission spectroscopy. Experimental and theoretical comparison will be made to our previous study and the difference the target gas makes on collisional activation will be discussed.

2. Methods

2.1. Experimental Methods. The CIE experiments were performed on a modified VG ZAB mass spectrometer. Originally a double-focusing mass spectrometer,[16,17] the third field-free region (3FFR) and the second electrostatic analyzer were later added to allow for mass spectrometric studies of fragment ions. The 3FFR and the instrumental setup for this work have been previously described.[15,18] Briefly, the 3FFR consists of a box 1 m long differentially pumped by two 6-in. diffusion pumps and ending in a second electrostatic analyzer. A deceleration−reacceleration collision cell assembly and a photon detection system consisting of a spectrograph (Acton SpectraPro 275, 27.5 focal length, 1200 g mm^{-1} holographic grating) and a thermoelectrically cooled charge-coupled device (CCD) detector (Andor DV401-UV, front-illuminated with UV coating) have been installed to the mass spectrometer for the detection of photon emissions resulting from ion-target collisions.

The $N_2^{+\bullet}$ ions are generated by electron ionization (with 80−90 eV electrons) in the ion source, mass selected by the magnetic analyzer, energy selected by the first electrostatic analyzer and collide with the target gas in the deceleration−reacceleration lens assembly at a collision gas pressure that reduces the precell ion flux by 10% (i.e., single collision condition).[2] Emissions from the excited ion beam and target gas were directly observed. The time window of observation ranges from 0.00−0.05 μs for 8 keV $N_2^{+\bullet}$ to 0.00−0.09 μs for 2 keV $N_2^{+\bullet}$, depending on the translational energy of the projectile ion. The entrance slit of the spectrograph is set to 3.0 mm to maximize emission signal intensity resulting in a spectral resolution of 8.5 nm (full width at half-height for atomic lines). Emission spectra were collected by the thermoelectrically cooled charge-coupled device (CCD) cooled to a temperature of −35

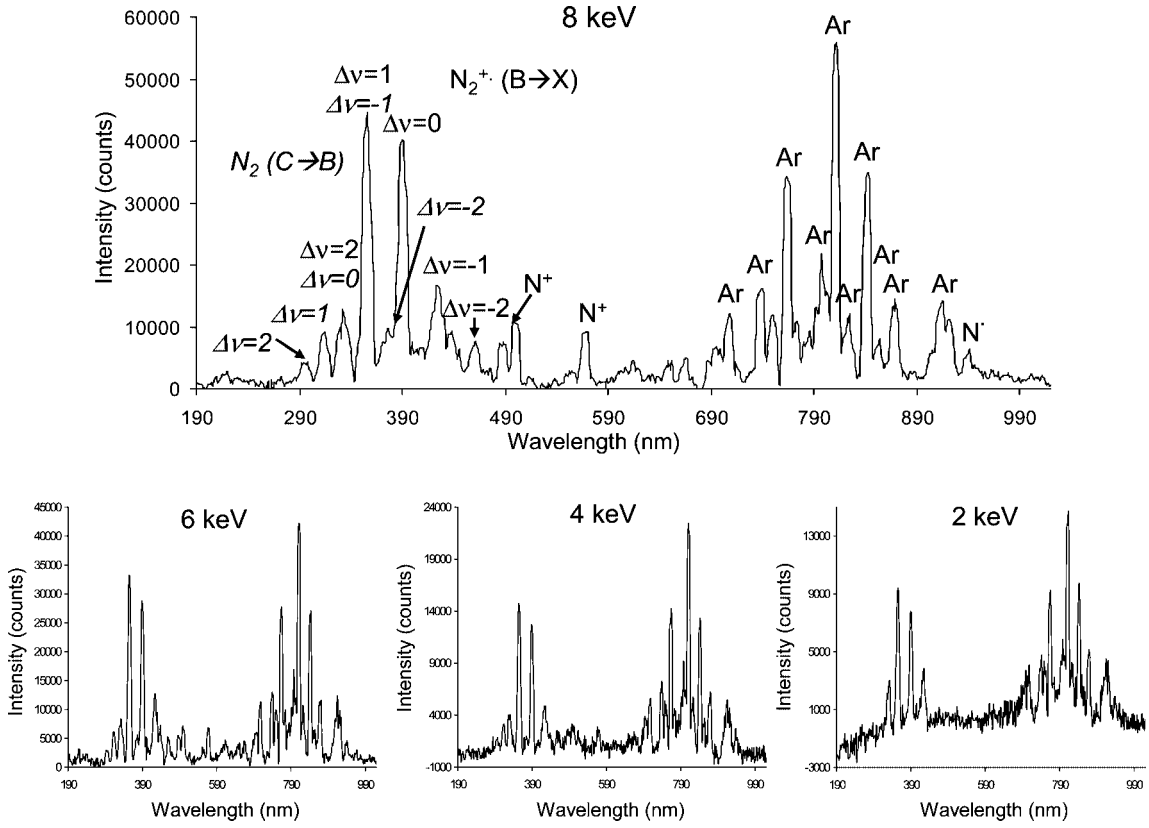

Figure 3. CIE spectra (190−1020 nm) of $N_2^{+\bullet}$/Ar collisions at different ion translational energies. All ion translational energies were obtained by varying the accelerating voltage at the ion source, except at 2 keV, which was obtained from a 3 keV ion beam with +1 kV applied to the collision cell. Collision gas pressure corresponded to 90% ion beam transmission. Peaks related to the N_2 C $^3\Pi_u \rightarrow$ B $^3\Pi_g$ transition are in italics.

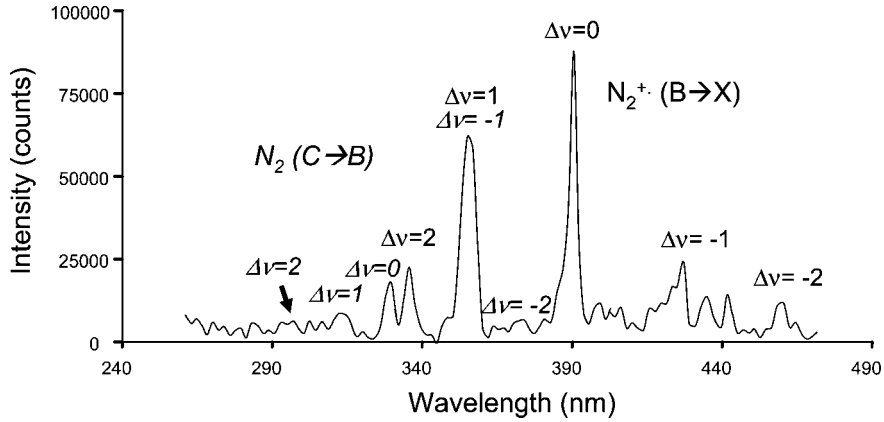

Figure 4. CIE spectrum (260−470 nm) of 8 keV $N_2^{+\bullet}$/Ar collisions obtained with an entrance slit width of 1.0 mm. The expected position of the $\Delta v = 2$ and $\Delta v = -2$ bands of the N_2 C $^3\Pi_u \rightarrow$ B $^3\Pi_g$ transition is labeled.

°C. Optical emissions from 190−1020 nm were recorded by the Andor MCD 2.63.1.8 program and were recorded in 14 separate segments, each being 50−70 nm wide. Two accumulations of 60 min were collected for each segment at full vertical binning reading mode, and each of the 14 segments was background subtracted. Background spectra were collected prior to signal acquisition at exactly the same conditions except without an ion beam. Spectral spikes resulting from cosmic rays were removed digitally by the program. Horizontal binning was performed manually in the ASCII file by combining data from every 20 pixel columns, and the overlapping portion of the spectrum at the two ends of each window was averaged.

A higher-resolution spectrum was collected from 260−470 nm following the above-described procedure except that the entrance slit width was narrowed to 1.0 mm and the data acquisition time of each accumulation was increased to 5 h. This resulted in a spectral resolution of 3.2 nm.

2.2. Theoretical Methods. Adiabatic potential energy curves for the collision complexes $N_2^{+\bullet}$−He and $N_2^{+\bullet}$−Ar as a function of collision coordinate were calculated at the CISD/6-311+G(2df) level of theory using the Gaussian 98 suite of programs.[19] Figure 2 shows the collision trajectory between a target atom and an $N_2^{+\bullet}$ ion as defined in our calculations. When the diatomic ion $N_2^{+\bullet}$ lies along the *y* axis, the collision trajectory of the target atom follows a path above and parallel to the *x* axis separated by β angstroms. Single-point energy calculations were performed as a function of α, from 0 to 3 Å (for He) and 4 Å (for Ar) in steps of 0.1 Å. Several trajectories with different β values were sampled (β varies from 0.5 to 0.8 Å for $N_2^{+\bullet}$/He and from 0.9 to 1.5 Å for $N_2^{+\bullet}$/Ar collisions). With the collision trajectory

as defined, the collision complex always possesses C_{2v} symmetry. This is obviously only one possible trajectory out of many, but we have chosen it because it forces the adiabatic curves to have different irreducible representations in the C_{2v} point group. They therefore correspond to the diabatic curves needed in the LZ model and allow us to determine which state crossings are mainly responsible for the excitation in the collisions. Since this representation of state crossings in the collision coordinate involves only conical intersections (due to symmetry), the value of H_{12} in eq 1 will always be zero and P will be 1, regardless of the slope differences between crossing states. It will be nonzero (which is needed to implement LZ theory) when the system deviates from C_{2v} symmetry (Table 1).

The potential energy curve of an electronic state of the complex may contain more than one individual orbital component. Π_u state, for example, consists of A_1 and B_1 components that may split into separate potential energy curves along the collision trajectory. Since both components yield similar potential energy curves from our calculations, especially at and near the crossing point, they will be presented as averaged results for each particular electronic state of the collision complex.

The potential energy curves of the $N_2^{+\bullet}-$He collision complex with $\beta = 0.8$ Å obtained from the CISD calculations were compared to that from time-dependent density function theory (TD B3-LYP/6-311+G(2df)). They both exhibit similar features (Figure S1, Supporting Information) and slope difference at the crossing points (Table 3).

3. Results and Discussion

3.1. $N_2^{+\bullet}$ Ion Beam. As discussed in our previous publication on $N_2^{+\bullet}$/He collisions,[15] an electron energy of 80−90 eV can produce $N_2^{+\bullet}$ in excited electronic states. However, on the basis of state lifetimes, ions that are formed initially in the B $^2\Sigma_u^+$ and C $^2\Sigma_u^+$ states will undergo spontaneous radiative decay to the ground state before arriving at the collision cell. Considerable $N_2^{+\bullet}$ A $^2\Pi_u$ may be involved in the collision events, but the fact that no $N_2^{+\bullet}$ A $^2\Pi_u \rightarrow$ X $^2\Sigma_g^+$ emissions could be detected in the absence of target gas suggest that the A $^2\Pi_u$ state makes up a negligible fraction of the ion beam.

3.2. Emission Spectra of $N_2^{+\bullet}$/Ar Collisions. The emission spectra over the wavelength range of 190−1020 nm obtained from $N_2^{+\bullet}$/Ar collisions at different projectile ion translational energies are presented in Figure 3. The prominent feature in the low wavelength region is the $\Delta\nu = +2, +1, 0, -1, -2$ vibrational transition progression of the $N_2^{+\bullet}$ B $^2\Sigma_u^+ \rightarrow$ X $^2\Sigma_g^+$ electronic transition. A vibrational transition progression in the N_2 C $^3\Pi_u \rightarrow$ B $^3\Pi_g$ electronic transition was also observed. Previously, when He was used as the target gas, the charge transfer process was unlikely because of the high ionization energy of He. A conversion of 9.01 eV from translational to internal energy is required for electron transfer to occur. To produce N_2(C) from charge transfer, 20.1 eV must be converted from translational to internal energy. In comparison, the charge transfer process with Ar is much more favorable. Only 0.18 eV is needed to produce N_2(X) and 11.3 eV to produce N_2(C).

The relative intensities of the N_2^+ B $^2\Sigma_u^+ \rightarrow$ X $^2\Sigma_g^+$ in Figure 3 appear to be different from what was observed from the $N_2^{+\bullet}$/He collisions[15] as the $\Delta\nu = 1$ peak is now the dominant peak in the vibrational progression. This results from the overlap of the N_2 and N_2^+ emissions as some of their wavelengths are very close. A higher-resolution spectrum with the entrance slit width reduced to 1.0 mm was obtained at this wavelength region, in an attempt to separate them (Figure 4). At this slit width, spectral resolution is increased to 3.2 nm. The $\Delta\nu = 0$ (at 330 nm) of N_2 C $^3\Pi_u \rightarrow$ B $^3\Pi_g$ and the $\Delta\nu = 2$ (at 335 nm) of N_2^+ B $^2\Sigma_u^+ \rightarrow$ X $^2\Sigma_g^+$ are obviously separated, but the peak at 355 nm is not. However, the peak intensity of $\Delta\nu = 1$ of N_2^+ B $^2\Sigma_u^+ \rightarrow$ X $^2\Sigma_g^+$ is now lower than that for $\Delta\nu = 0$. This now better resembles the $N_2^{+\bullet}$/He spectrum and may indicate that the two peaks are on the verge of separation.

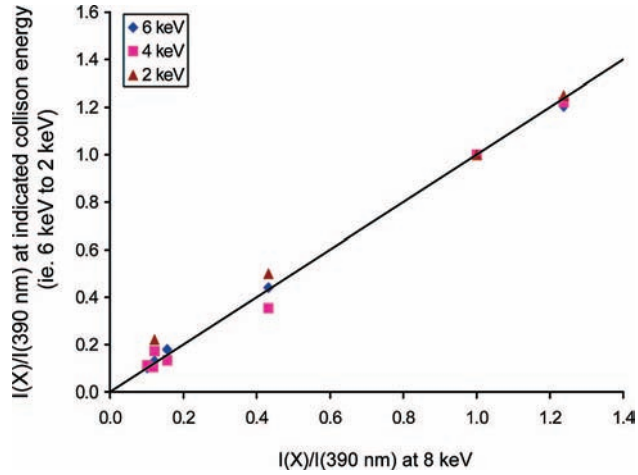

Figure 5. Lifetime-corrected plot of the relative emission intensities of $N_2^{+\bullet}$, N^+, and $N^\bullet$ at various ion translational energies versus those at 8 keV. I(X) represents the intensity of $N_2^{+\bullet}$, N^+, and $N^\bullet$ and I(390 nm) the intensity of the B $^2\Sigma_u^+ \rightarrow$ X $^2\Sigma_g^+$ ($\Delta\nu = 0$) transition of $N_2^{+\bullet}$.

At 2 keV ion translational energy, N_2 C $^3\Pi_u \rightarrow$ B $^3\Pi_g$ emissions were not observed. Kelley et al. studied emissions (310−435 nm) from $N_2^{+\bullet}$/Ar collisions with $N_2^{+\bullet}$ translational energy ranges from 100 eV to 1 keV.[20] Within this energy range, no N_2 C $^3\Pi_u \rightarrow$ B $^3\Pi_g$ was observed. This indicates that at low translational energy, the probability of forming N_2 C $^3\Pi_u$ is small, precluding our observation of the weak $\Delta\nu = 2, 1$ bands at 2 keV.

The emissions from the excited N^+ fragments resulting from the dissociation of $N_2^{+\bullet}$ can also be observed, but those from the excited $N^\bullet$ are not obvious. This is because of the presence of many intense peaks from Ar in the high wavelength region. The only unambiguous $N^\bullet$ peak (i.e., free from Ar interference) is the (3p) $^2D^0 \rightarrow$ (3s) ^2P transition observed at 941 nm.

Similar to the $N_2^{+\bullet}$/He collisions, the relative intensities of the spectral peaks were also compared. The relative intensity has been corrected for the difference in lifetime of the various states since we only observe a portion of the emission from the excited-state species. Figure 5 presents the relative intensity plot when all collisions were assumed to take place when they enter the observation region (i.e., near the center of the collision cell). All the points fall along the $y = x$ line, indicating that the relative intensities from $N_2^{+\bullet}$, N^+, and $N^\bullet$ do not change with ion translational energy, consistent with the curve-crossing mechanism. Relative intensity plots without lifetime correction and with a different lifetime correction can be found in Figure S2 in Supporting Information for comparison. It leads to the same conclusion as our previous study on $N_2^{+\bullet}$/He collisions in which the vast majority of collision events take place under the observation window. The intensities of the emissions from the target gas cannot be directly compared with those from the projectile ions or fragments since the spatial distribution of collisions across the collision cell is unknown.

3.3. Comparison of $N_2^{+\bullet}$/He and $N_2^{+\bullet}$/Ar Collisions. The $N_2^{+\bullet}$ B $^2\Sigma_u^+ \rightarrow$ X $^2\Sigma_g^+$ emission intensities of keV $N_2^{+\bullet}$/He

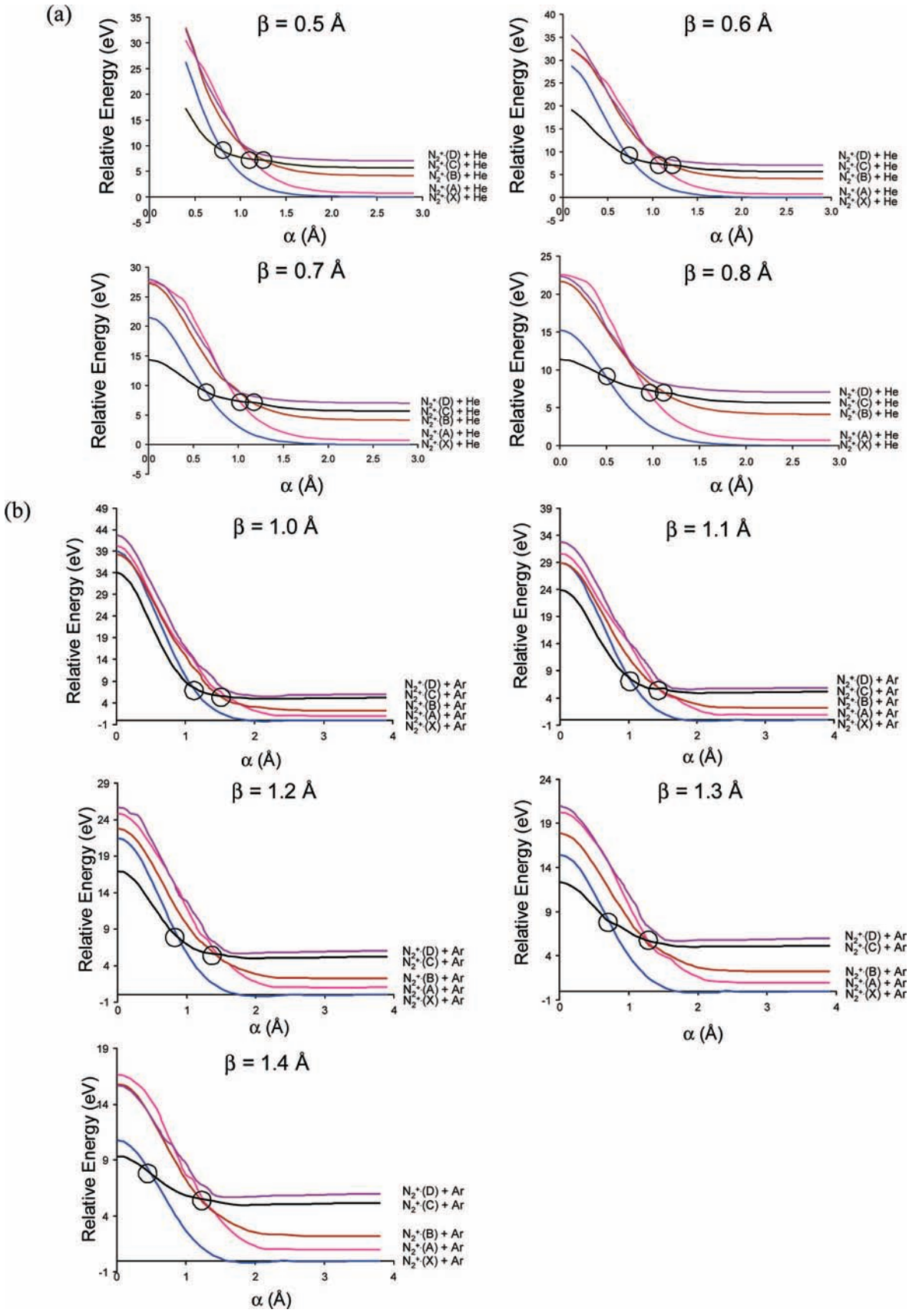

Figure 6. Adiabatic potential energy curves of the (a) $N_2^{+\bullet}$−He and (b) $N_2^{+\bullet}$−Ar collision complexes at various β values calculated at the CISD/6-311+G(2df) level of theory. The location of the crossing points is circled.

and $N_2^{+\bullet}$/Ar collisions at 90% beam transmission were compared. Table 2 tabulates the photon counts of the peak at 356 nm ($\Delta\nu = +1$) and 390 nm ($\Delta\nu = 0$) arising from both types of collisions. Emissions were collected with an accumulation time of 30 min and 1 h. It is clear that $N_2^{+\bullet}$/He collisions result in emission intensities that is about four times stronger (based

on $\Delta v = 0$). The difference could not have been caused by ion scattering. Even though a stronger scattering effect would be expected with argon, comparison of scattering cross sections of $O^{\bullet}$ by He and Ar shows that 99% and 98%, respectively would have exited the collision cell.[21] This difference is too small to have any significant impact on the emission intensities. The charge-transfer process can also reduce the amount of $N_2^{+\bullet}$ B $^2\Sigma_u^+$ state being formed. In order for the signal to decrease by 2−4 times, 50−75% of the $N_2^{+\bullet}$ ion beam needs to be neutralized upon collisions. A careful neutralization-reionization study of $N_2^{+\bullet}$ found that the charge transfer efficiency between $N_2^{+\bullet}$ and Ar is only about 5%.[22]

Figure 6 presents the adiabatic potential energy curves of the $N_2^{+\bullet}$−He and $N_2^{+\bullet}$−Ar collision complex at different β values calculated at the CISD/6-311+G(2df) level of theory. As the excited states of He and Ar are higher in energy than those of $N_2^{+\bullet}$, the lowest excited states of the collision complex are composed of the interaction of the ground-state of He or Ar with various electronic states of $N_2^{+\bullet}$. A small dip (~0.2 eV) is observed in the $N_2^{+\bullet}$−Ar potential energy curves at around 2.1 Å. This indicates that there is a small attractive potential between Ar and N_2^+ and is in agreement with other computational and spectroscopic studies of the N_2^+−He and N_2^+−Ne complexes.[23]

In all cases, the $N_2^{+\bullet}$ X $^2\Sigma_g^+$ state crosses with only the C $^2\Sigma_u^+$ state, not the A $^2\Pi_u$ or B $^2\Sigma_u^+$ state. Therefore, excitation to the B $^2\Sigma_u^+$ state will normally require curve-crossing first to the C $^2\Sigma_u^+$ state and then from the C $^2\Sigma_u^+$ state to the B $^2\Sigma_u^+$ state. This result agrees with translational energy loss experiments in which the C $^2\Sigma_u^+$ state was identified as the most important transitions involved in the production of N^+.[12,13]

As a result of nuclear and electronic interactions, a lower β (i.e., smaller impact parameter) leads to crossing at a larger collision distance. As a result, the ion-target distance (d) (see Figure 2) and the potential energy at the crossing point is almost constant with respect to β. According to the Landau−Zener model, the probability (P) of crossing over to another electronic state is reflected in terms of the Hamiltonian for the crossing, H_{12}, the slope difference at the crossing point and the ion velocity (equation 1). In the two collision systems, excitation of the collision complex occurs initially by the crossing from the ground electronic state to the excited-state corresponding to the C $^2\Sigma_u^+$ state of $N_2^{+\bullet}$. If we make the assumption that the H_{12} terms for this transition in the two collision systems will be similar (since the same states of $N_2^{+\bullet}$ are involved and they both correspond to single electronic excitations), differences in the transition probability will be dictated mostly by the slope difference at the crossing point between the two diabatic curves. The same assumption could be made for the C $^2\Sigma_u^+$ to B $^2\Sigma_u^+$ state crossing (which represents a two-electron state change) in the two collision systems. Larger differences in slope represent a higher probability of crossing-over. A comparison was therefore made of the slope differences at different β parameters for both collision systems (Table 3) within the C_{2v} symmetry constraint of our model. The slope differences at the X−C crossing point are larger for $N_2^{+\bullet}$/He than for $N_2^{+\bullet}$/Ar, whereas those at the C−B crossing point are similar in both cases. On the basis of this picture, the formation of ions in the B $^2\Sigma_u^+$ state is more probable in $N_2^{+\bullet}$/He collisions because more ions first cross over to the C $^2\Sigma_u^+$ state upon collision with the He target and then subsequently cross to the B $^2\Sigma_u^+$ state.

Another observation is that we see relatively more fragment emissions versus B $^2\Sigma_u^+ \rightarrow$ X $^2\Sigma_g^+$ emissions in collisions with Ar as compared to collisions with He. This agrees with conclusions from Martinez and Fuentes, who measured higher dissociation cross sections for $N_2^{+\bullet}$/Ar collisions.[12,24]

4. Conclusions

This paper compares the collision-induced emissions from keV $N_2^{+\bullet}$/He and $N_2^{+\bullet}$/Ar collisions and presents evidence that supports the curve-crossing mechanism for collisional activation. First, the excited-state species formed as a result of high keV $N_2^{+\bullet}$/Ar collisions were probed by collision-induced emission spectroscopy. The relative population of electronically excited $N_2^{+\bullet}$, N^+, and $N^{\bullet}$ states remains constant as the collision energy is increased from 2 to 8 keV. This result is consistent with the curve-crossing mechanism in which increasing collision energy in the keV energy range increases the probability of crossing from one potential curve to another at the crossing points; therefore, the overall population in the excited states increases but the same relative population among the excited states could result. Second, the role of the target gas in $N_2^{+\bullet}$/He and $N_2^{+\bullet}$/Ar collisions was compared by emission spectroscopy and theoretical calculations. Adiabatic potential energy surfaces for $N_2^{+\bullet}$/He and $N_2^{+\bullet}$/Ar collisions indicate that the ground state of $N_2^{+\bullet}$ does not cross directly with the A $^2\Pi_u$ or B $^2\Sigma_u^+$ state. Rather, it involves curve-crossing first to the C $^2\Sigma_u^+$ state. The difference in emission intensities from the B $^2\Sigma_u^+ \rightarrow$ X $^2\Sigma_g^+$ emission of $N_2^{+\bullet}$ in the two systems can be accounted for by the slope differences in the adiabatic potential energy surfaces based on the Landau−Zener curve-crossing model.

Acknowledgment. The authors thank the Natural Sciences and Engineering Research Council (NSERC) of Canada for continuing financial support and the referee for key advice on how to improve the manuscript. C.P. thanks NSERC for a postgraduate scholarship during the tenure of which this work is completed.

Supporting Information Available: Adiabatic potential energy curves and plots of the relative emission intensities. This material is available free of charge via the Internet at http://pubs.acs.org.

References and Notes

(1) Cooks, R. G. *Collision Spectroscopy*; Plenum Press: New York, 1978.
(2) Holmes, J. L. *Org. Mass Spectrom.* **1985**, *20*, 169.
(3) Levsen, K.; Schwarz, H. *Mass Spectrom. Rev.* **1983**, *2*, 77.
(4) Todd, P. J.; McLafferty, F. W. *Tandem Mass Spectrometry*, Wiley-Interscience: New York, 1983.
(5) Durup, J. Recent developments in mass spectrometry. In *Mechanisms of Collision-Induced Dissociation of Fast Ions*; Ogata, K., Hayakawa, T., Eds.; University of Tokyo Press: Tokyo, 1970.
(6) McLuckey, S. A. *J. Am. Soc. Mass Spectrom.* **1992**, *3*, 599.
(7) Massey, H. S. W.; Burhop, E. H. S. *Electronic and Ionic Impact Phenomena*; Clarendon Press: Oxford, 1952.
(8) Note that the *h* in eq 1 has been placed in the denominator instead of the numerator as in ref 7, p 446. It is a typo in ref 7.
(9) Nikitin, E. E. *Theory of Elementary Atomic and Molecular Processes in Gases*; Clarendon Press: Oxford, 1974.
(10) Desouter-Lecomte, M.; Dehareng, D.; Leyh-Nihant, B.; Praet, M. Th.; Lorquet, A. J.; Lorquet, J. C. *J. Phys. Chem.* **1985**, *89*, 214.
(11) Brenton, A. G. *Int. J. Mass Spectrom.* **2000**, *200*, 403.
(12) Fuentes, B. E.; Martinez, H. *Int. J. Mass Spectrom.* **2004**, *238*, 55.
(13) Fournier, P.; VandeRunstraat, C. A.; Govers, T. R.; Schopman, J.; deHeer, F. J.; Los, J. *Chem. Phys. Lett.* **1971**, *9*, 426.
(14) Leventhal, J. J. The emission of light from excited products of charge exchange reactions. In *Gas Phase Ion Chemistry*; Bowers, M. T., Ed.; Academic Press: Orlando, 1984; Vol. 3.
(15) Poon, C.; Mayer, P. M. *J. Phys. Chem. A* **2007**, *111*, 777.
(16) Burgers, P. C.; Holmes, J. L.; Szulejko, J. E.; Mommers, A. A.; Terlouw, J. K. *Org. Mass Spectrom.* **1983**, *18*, 254.
(17) Holmes, J. L.; Mommers, A. A.; Terlouw, J. K.; Hop, C. E. C. A. *Int. J. Mass Spectrom. Ion Processes* **1986**, *68*, 249.

(18) Holmes, J. L.; Mayer, P. M.; Mommers, A. A. *Int. J. Mass Spectrom. Ion Processes* **1994**, *135*, 213.

(19) Frisch, M. J.; Trucks, G. W.; Schlegel, H. B.; Scuseria, G. E.; Robb, M. A.; Cheeseman, J. R.; Zakrzewski, V. G.; Montgomery, J. A.; Stratmann, R. E.; Burant, J. C.; Dapprich, S.; Millam, J. M.; Daniels, A. D.; Kudin, K. N.; Strain, M. C.; Farkas, O.; J. Tomasi; Barone, V.; Cossi, M.; Cammi, R.; Mennucci, B.; Pomelli, C.; Adamo, C.; Clifford, S.; Ochterski, J.; Petersson, G. A.; Ayala, P. Y.; Cui, Q.; Morokuma, K.; Malick, D. K.; Rabuck, A. D.; Raghavachari, K.; Foresman, J. B.; Cioslowski, J.; Ortiz, J. V.; Stefanov, B. B.; Liu, G.; Liashenko, A.; Piskorz, P.; Komaromi, I.; Gomperts, R.; Martin, R. L.; Fox, D. J.; Keith, T.; Al-Laham, M. A.; Peng, C. Y.; Nanayakkara, A.; Gonzalez, C.; Challacombe, M.; Gill, P. M. W.; Johnson, B.; Chen, W.; Wong, M. W.; Andres, J. L.; Gonzalez, C.; Head-Gordon, M.; Replogle, E. S.; Pople, J. A. *GAUSSIAN 98 Rev. A.6*; Gaussian, Inc.: Pittsburgh, PA, 1998.

(20) Kelley, J. D.; Bearman, G. H.; Harris, H. H.; Leventhal, J. J. *J. Chem. Phys.* **1978**, *68*, 3345.

(21) Smith, G. J.; Gao, R. S.; Lindsay, B. G.; Smith, K. A.; Stebbings, R. F. *Phys. Rev. A* **1996**, *53*, 1581.

(22) Rennie, E. E.; Mayer, P. M. *J. Chem. Phys.* **2004**, *120*, 10561.

(23) Maier, J. P. *Mass Spectrom. Rev.* **1992**, *11*, 119.

(24) Martinez, H.; Fuentes, B. E. *Nucl. Instrum. Methods Phys. Res., Sect. B* **2005**, *241*, 459.

(25) Bennett, R. G.; Dalby, F. W. *J. Chem. Phys.* **1959**, *31*, 434.

(26) Hesser, J. E.; Dressler, K. *J. Chem. Phys.* **1966**, *45*, 3149.

(27) Lofthus, A.; Krupenie, P. H. *J. Phys. Chem. Ref. Data* **1977**, *6*, 113.

(28) Dumont, M. N.; Remy, F. *J. Chem. Phys.* **1982**, *76*, 1175.

(29) Bashkin, S.; Stoner, J. O. *Atomic Energy Levels & Grotrian Diagrams 1*; North-Holland Publishing Company: New York, 1975.

(30) Wiese, W. L.; Smith, M. W.; Glennon, B. M. *Atomic Transition Probabilities*; National Bureau of Standards: Washington, DC, 1966; Vol. I.

(31) Norlen, G. *Phys. Scr.* **1973**, *8*, 249.

JP8017524